


ORIGINAL PAPER

Open Access



Class II phosphatidylinositol 3-kinase α and β isoforms are required for vascular smooth muscle Rho activation, contraction and blood pressure regulation in mice

Shahidul Islam¹, Kazuaki Yoshioka¹, Sho Aki¹, Kazuhiro Ishimaru¹, Hiroki Yamada¹, Noriko Takuwa^{1,2} and Yoh Takuwa^{1*} 

Abstract

Class II phosphatidylinositol 3-kinases (PI3K), PI3K-C2 α and PI3K-C2 β , are involved in cellular processes including endocytosis, cilia formation and autophagy. However, the role of PI3K-C2 α and PI3K-C2 β at the organismal level is not well understood. We found that double knockout (KO) mice with both smooth muscle-specific KO of PI3K-C2 α and global PI3K-C2 β KO, but not single KO mice of either PI3K-C2 α or PI3K-C2 β , exhibited reductions in arterial blood pressure and substantial attenuation of contractile responses of isolated aortic rings. In wild-type vascular smooth muscle cells, double knockdown of PI3K-C2 α and PI3K-C2 β but not single knockdown of either PI3K markedly inhibited contraction with reduced phosphorylation of 20-kDa myosin light chain and MYPT1 and Rho activation, but without inhibition of the intracellular Ca²⁺ mobilization. These data indicate that PI3K-C2 α and PI3K-C2 β play the redundant but essential role for vascular smooth muscle contraction and blood pressure regulation mainly through their involvement in Rho activation.

Keywords: Class II phosphatidylinositol 3-kinase, Vascular smooth muscle, Contraction, Rho, Blood pressure

Introduction

Phosphatidylinositol 3-kinases (PI3K) are lipid kinases that catalyze the phosphorylation of phosphoinositides at the D3 position of their inositol ring and, thereby, control a diverse array of cellular processes including vesicular trafficking, cell migration, cell proliferation and cell metabolism [1]. Mammals possess eight PI3K isoforms, which are divided into three classes (class I, II and III), based on their structural homology, substrate specificity and mode of regulation [2]. Class I PI3K are activated

downstream of various receptor tyrosine kinases and G protein-coupled receptors to mainly generate phosphatidylinositol-3,4,5-trisphosphates and to mediate cell proliferation, survival, and migration. Through these effects, class I PI3K are involved in cancer and allergic diseases. The unique member of class III, Vps34, is responsible for a significant fraction of phosphatidylinositol-3-monophosphate in autophagosomes and endosomes, in which it controls the formation of phagophores as well as docking and fusion of endosomes. Class II PI3K, which comprises three isoforms PI3K-C2 α (C2 α), PI3K-C2 β (C2 β) and PI3K-C2 γ , mainly produce phosphatidylinositol-3,4-bisphosphate (PI(3,4)P₂) and are involved in endocytosis, autophagy and cilia formation at the cellular level [3–8]. C2 α and C2 β are ubiquitously expressed widely in various organs and tissues whereas PI3K-C2 γ

*Correspondence: ytakuwa@med.kanazawa-u.ac.jp

¹ Department of Physiology, Kanazawa University Graduate School of Medical Sciences, 13-1 Takara-machi, Kanazawa, Ishikawa 920-8640, Japan

Full list of author information is available at the end of the article



expression is restricted mainly in liver, breast, testis and prostate [9]. C2 β is highly homologous in its amino acid sequence to C2 α and exhibits similar activities including cell migration and growth to those of C2 α . However, the physiological function of class II PI3K is still poorly understood compared with class I and class III PI3K.

We previously showed that C2 α , which is clearly less sensitive to the PI3K inhibitors wortmannin and LY294002 [10, 11], was required for membrane depolarization- and receptor agonist-induced contraction of isolated blood vessel strips and vascular smooth muscle cells [12–14]. Moreover, our study suggested that C2 α was involved in Rho activation and Rho kinase-dependent phosphorylation of the myosin-targeting subunit MYPT1 of myosin light chain phosphatase (MLCP) and, thereby, an increase in phosphorylation of 20 kDa regulatory myosin light chain (MLC₂₀). We further demonstrated that in vascular smooth muscle of spontaneously hypertensive rats, enhanced activation of C2 α contributed to increased Rho activity, elevated vascular tone and hypertension [15]. These observations suggested that C2 α is an important regulatory molecule for Rho activation and contraction in vascular smooth muscle.

In order to better understand the role of C2 α at the organismal level, we generated C2 α -knockout (KO) mice and analyzed their phenotype. Global C2 α -homozygous KO mice were embryonic lethal owing to severe defects of angiogenesis [3]. Endothelial-specific genetic deletion of C2 α recapitulated this phenotype. In contrast to C2 α , global C2 β -homozygous KO mice were apparently normal [16]. We, therefore, generated smooth muscle-specific C2 α -deleted mice with or without global C2 β KO to study the role of C2 α and C2 β in vascular smooth muscle contraction. Our data show that single KO of either C2 α or C2 β did not affect vascular smooth muscle contraction or blood pressure, but that double KO of C2 α and C2 β resulted in markedly attenuated vascular smooth muscle contraction with impaired Rho activation and decreased blood pressure compared with control mice. These observations indicate that C2 α and C2 β have the essential compensatory role for vascular smooth muscle contraction and blood pressure regulation in mice.

Methods

Mice

Mice were housed in a temperature-controlled (24 °C) facility room under a 12-h/12-h light–dark cycle with free access to regular chow and water under specific pathogen-free conditions in the animal facility of the University of Kanazawa. All mouse experiments were performed following the “fundamental guidelines for proper conduct of animal experiment and related activities in academic research institutions” under the jurisdiction of

the Ministry of Education, Culture, Sports, Science, and Technology of Japan and were approved by the Committee on Animal Experimentation of Kanazawa University. PI3K-C2 α -floxed (C2 α ^{flox/flox}) mice, PI3K-C2 β -null (C2 β ^{-/-}) mice, and Rosa26-CAG-loxP-stop-loxP-tdTomato (R26-tdTomato) reporter mice were described previously [3, 17]. To generate smooth muscle-specific conditional C2 α -KO mice, C2 α ^{flox/flox} mice were crossed with SM22 α -Cre transgenic mice (# 004746, Jackson Lab.). To evaluate Cre-mediated recombination efficiency, SM22 α -Cre; R26-tdTomato mice were generated. Mice were euthanized using intraperitoneal injections of overdoses of three combined anesthetics, medetomidine (ZENOAQ, Fukushima, Japan), midazolam (Astellas, Tokyo, Japan) and butorphanol (Meiji Seika Pharma, Tokyo, Japan) according to the acceptable euthanasia guidelines. Mice were genotyped by PCR analysis of genomic DNA prepared from tail biopsies.

Immunofluorescent staining of aortic sections

The perfusion-fixed aortae were embedded in Tissue-Tek OCT compound (Sakura Finetek, Tokyo, Japan), and the prepared sections were blocked with phosphate buffer saline containing 0.1% Triton X-100, 0.1% Tween 20, 1% bovine serum albumin, and 5% non-immune goat serum for 1 h at room temperature. The cryosections of aorta were subjected to immunofluorescent staining using the following primary antibodies: mouse monoclonal anti- α SMA (#A5228, Sigma-Aldrich, St. Louis, MO, USA), mouse monoclonal anti-SM22 α (#ab10135; Abcam, Cambridge, UK), rabbit polyclonal anti-smooth muscle myosin heavy chain 11 (#ab53219; Abcam), rabbit polyclonal anti-C2 α (#AP11855B, Abgent, San Diego, CA, USA), rabbit polyclonal anti-C2 β (#sc-134766, Santa Cruz Biotechnology, Dallas, TX, USA). The sections were treated with appropriate Alexa-Fluor conjugated secondary antibodies (Molecular Probes) and, then, mounted with 4',6-diamidino-2-phenylindole (DAPI) for nuclear staining.

Measurement of blood pressure

Male mice aged 10 to 12 weeks were used. Mice were trained by repeated blood pressure measurements in several trials until the basal condition was stabilized and the consistent and stable reading was monitored. The systolic, diastolic and mean blood pressure with the heart rate of conscious mice was recorded using a tail-cuff system (Softron, Tokyo, Japan) as reported previously [15, 18].

Measurements of isometric tension of aortic rings

The aorta was isolated from control and DKO mice aged 10 to 12 weeks, cleaned free of adhering connective

tissues and cut into rings of 3–4 mm width in ice-cold modified Krebs–Henseleit buffer as previously described [12, 14]. Aortic rings were placed in contraction chambers at 37 °C under the aeration with 95% O₂ and 5% CO₂, and isometric tension was determined with a transducer (#UFERUM-203, Kishimoto Medical Instruments, Kyoto, Japan) as described previously [12, 14]. Aortic rings were stimulated with various doses of KCl and noradrenaline (NA) (Cayman Chemical) in cumulative manners. When indicated, aortic rings were pretreated with the Rho kinase inhibitor Y-27632 (10 μM) (FUJIFILM Wako Pure Chemical, Osaka, Japan). After tension measurements, aortic rings were fixed in 4% formalin overnight at 4 °C and embedded in paraffin, followed by cross-sectioning and Azan staining for the determination of the medial smooth muscle area. Tensions were corrected by a cross-sectional medial smooth muscle area in each aortic ring.

Plasmids

The enhanced green fluorescent protein (GFP)-tagged human PI3K-C2α (GFP-C2α) expression vector was previously described [3]. Human PI3K-C2β cDNA was obtained from K. Kitatani (Setsunan University) [19]. To generate mCherry-tagged PI3K-C2α (mCherry-C2α) and GFP- and mCherry-tagged PI3K-C2β (GFP-C2β and mCherry-C2β), human PI3K-C2α and PI3K-C2β cDNA fragments were amplified by PCR using Prime STAR HS DNA Polymerase (Takara, Shiga, Japan) and sub-cloned into pmCherry-C1 (Takara) and pAcGFP1-N vectors (Clontech, Mountain View, CA, USA), using the In-Fusion HD Cloning kit (Clontech). The plasmid vectors of RhoA-FRET sensor, pTriEx-RhoA-wt_mScarlet-i_SGFP2 (#85071, Addgene), and BFP-Rab5 (#49147; Addgene) were obtained from Dorus Gadella and Gia Voeltz, respectively, through Addgene.

Aortic smooth muscle cells

Mouse aortic smooth muscle cells (MASM) were isolated from 4-week-old mouse aortae by an enzyme-dispersion method. Briefly, aortae were dissected under sterile conditions and incubated at 37 °C in 0.1% collagenase (Type II) (#LS004202, Worthington Biochemical, Lakewood, NJ, USA), 0.75 unit/mL elastase (Type III) (#LS002279, Worthington Biochemical) and 0.1% trypsin inhibitor (#LS003570, Worthington Biochemical) for 30 min, followed by further incubation of the mixtures for 60 min after separating the adventitia from aortae. Dispersed single cells were separated from undigested tissues by filtration through Cell Strainers (100 μm) (#352360, BD Falcon) and collected by centrifugation at 500g for 5 min. Cells thus obtained were plated onto laminin (20 μg/mL in PBS) (FUJIFILM Wako Pure Chemical Corp. Cat no. 120-05751)-coated glass bottom dishes (MatTek,

Bratislava, Slovakia) with the growth medium SmGM-2, which contains 5% fetal bovine serum (FBS) and growth factor supplements (#CC-3182, Lonza, Walkersville MD, USA). Human aortic smooth muscle cells (HASM), which were purchased from Lonza (#CC-2571, Lonza), were also plated onto laminin-coated dishes and slides with SmGM-2. After cells were cultured for 3 to 4 days, cells were transfected with siRNAs and Lipofectamine RNAiMAX (Invitrogen/Thermo Fisher Scientific) in Opti-MEM (Invitrogen/Thermo Fisher Scientific) by incubating cells with siRNA was 4 to 6 h and cultured in SmGM2 for 48 h. The concentrations of siRNAs were 50 nM for the transfection of a single siRNA (single transfection) and 25 nM each for the transfection of two siRNAs (double transfection). Our preliminary studies confirmed that 25 and 50 nM of siRNAs in the single transfection and 25 nM of siRNAs in the double transfection gave the similar extents of inhibition of protein expression of our interest. The targeted sequences of siRNA were: 5'-AAG GUU GGC ACU UAC AAG AAU-3' for human PI3K-C2α and 5'-AAG CCG GAA GCU UCU GGG UUU-3' for human PI3K-C2β. The control siRNA sequence was 5'-AAU UCU CCG AACGUG UCA CGU-3'. We transfected cells with GFP- and mCherry-tagged PI3K expression vectors using Lipofectamine (Invitrogen/Thermo Fisher Scientific) in Opti-MEM, followed by cultures in the growth medium for 3–4 days. Cells were serum- and growth factor-starved for 1 to 4 h in DMEM supplemented with 0.1% fatty acid free BSA (Sigma-Aldrich) for contraction assay, Western blot analyses of phosphorylation of MLC₂₀ and MYPT1, and Rho imaging analyses.

Determinations of contraction and the intracellular free Ca²⁺ concentration ([Ca²⁺]_i) of vascular smooth muscle cells

Cells were loaded with the fluorescent Ca²⁺ indicator fluo-8 acetoxymethylester (AM) (2.5 μM) (Molecular Probes) in Hank's Balanced Salt Solution (HBSS) for 30 min in the dark at 37 °C, followed by 1 h starvation with serum-free, phenol red-free FluoroBrite DMEM (Gibco, Thermo Fisher Scientific). After cells were washed with FluoroBrite DMEM two times, cells were imaged in FluoroBrite DMEM at 37 °C using a confocal microscope (inverted IX70 microscope; Olympus Corp., Tokyo, Japan) equipped with a confocal disk-scanning unit (CSU10, Yokogawa, Tokyo, Japan) as described previously [13]. The acquisition and process were controlled by iQ software (Andor, Belfast, UK). For evaluations of cell contraction, a stimulus-induced reduction in the planar cell surface area, which was sharply visualized by fluo-8 fluorescence, was determined and expressed as a stimulus-induced change (ΔA) of the planar cell area over

the planar cell area before stimulation (A_0) [12, 13]. A stimulus-induced change in the $[Ca^{2+}]_i$ was determined using the fluorescent Ca^{2+} indicator Fluo-8 as described previously [13]. Changes in Fluo-8 fluorescence were monitored every 10 s with excitation at 488 nm light and emission fluorescence at 510 nm. The ratio of ionomycin-stimulated fluorescence intensity over basal intensity was calculated.

Fluorescence resonance energy transfer (FRET) imaging for Rho activation

For FRET imaging analysis, HASM were transfected with the RhoA-FRET sensor probe [3, 17] using an Amaxa Nucleofector system (Lonza) and plated onto laminin-coated, glass-bottomed culture dishes. For the measurements of RhoA-FRET signals, the ratio imaging was carried out on the Dragonfly confocal system (Andor) equipped with the Andor's spinning-disk unit and EMCCD camera (iXon DU888) based on an inverted Nikon Eclipse Ti2 microscope (Nikon Instrument, Tokyo Japan). Cells were stimulated with either ionomycin (IMC) (0.3 μ M) or endothelin-1 (ET-1) (1 μ M), after 2 min observations as baseline signals. Pseudo-color ratio images were generated from images from GFP and FRET channels using Andor iQ software. RhoA-FRET signal intensity within ten subcellular regions per cell at 3 min after the addition of agonists was quantified. The ratio of ionomycin- and endothelin-stimulated fluorescence intensity/basal intensity was expressed. In some experiments, the co-localization of RhoA-FRET signals and blue fluorescent protein–Rab5 signals was evaluated.

Immunofluorescence staining of cells

HASM were cultured in SmGM2 at 37 °C under 5% CO_2 . Cells of the passage number between 5 and 6 were used for experiments. Cells were rinsed with Dulbecco's phosphate-buffered saline (PBS) once and fixed with 4% paraformaldehyde in 0.1 M phosphate buffer (pH 7.4) for 10 min at room temperature, followed by permeabilization with 0.3% TritonX-100 in PBS for 15 min or with 90% chilled methanol for 5 min. After blocking in 5% normal goat serum (FUJIFILM Wako Pure Chemical Corp.) and 0.3% TritonX-100 in PBS, cells were incubated with rabbit polyclonal anti-clathrin heavy chain (1:400) (#ab21679, Abcam) overnight at 4 °C. After washing, cells were incubated with an appropriate Alexa-Fluor-conjugated secondary antibody (Molecular Probes) for 1 h at room temperature.

Immunoblot analyses

Cells were quickly washed with PBS 48–72 h after siRNA transfection and scraped into either 2× Laemmli's SDS sample buffer or the RIPA lysis buffer on ice. For

determination of MLC_{20} and MYPT1 phosphorylation, cells were quickly rinsed and quenched by adding an ice-cold stop buffer containing 10% trichloroacetic acid, 150 mM NaCl, 2 mM DTT and 4 mM EGTA, followed by scraping into 2× Laemmli's SDS sample buffer. The pH of cell lysates was neutralized by adding a concentrated Tris solution. Cell lysates were then boiled for 5 min and centrifuged for 5 min at 15,000 rpm. The resultant supernatants were separated on 8 to 15% SDS-PAGE, followed by electro-transfer onto polyvinylidene difluoride membranes (Immobilon-P, Millipore-Merck, Nottingham, UK) using the Trans-Blot Turbo blotting system (Bio-Rad, Hercules, CA, USA). After blocking, membranes were incubated with primary antibodies at 4 °C overnight. The antibodies used were: rabbit monoclonal anti-PI3K-C2 α (1:1000) (#12402; CST), mouse monoclonal anti-PI3K-C2 β (1:500) (#611342, BD Biosciences, San Diego, CA USA), rabbit polyclonal anti-Mhc11 (1:1000) (#ab53219; Abcam), monoclonal anti-20 kDa myosin light chain (MLC_{20}) (1:1000) (#M4401, Sigma-Aldrich), rabbit polyclonal anti-phospho- MLC_{20} (Ser¹⁹) (1:500) (#3671, CST), rabbit polyclonal anti-phospho- MLC_{20} (Thr¹⁸/Ser¹⁹) (1:500) (#3674, CST), mouse monoclonal anti-myosin light chain kinase (MLCK) (1:1000) (#M7905, Sigma-Aldrich), mouse monoclonal anti-MYPT1(1:1000) (#612165, BD Biosciences), rabbit polyclonal anti-phosphorylated MYPT1 (Thr⁸⁵³) (1:1000) (#4563, CST), mouse monoclonal anti-smooth muscle-specific α -actin (α SMA) (1:1000) (#A5228, Sigma-Aldrich), mouse monoclonal anti-glyceraldehyde 3-phosphate dehydrogenase (GAPDH) (1:1000) (#016-25523, FUJIFILM-Wako Pure Chemical), and mouse monoclonal anti- β -actin (1:1000) (#010-27841, FUJIFILM-Wako Pure Chemical). Membranes were then incubated with alkaline phosphatase-conjugated secondary antibodies, anti-rabbit immunoglobulin (Ig) G antibody (1:1000) (#7054, CST) and anti-mouse IgG antibody (1:1000) (#7056, CST) for 1 h, and the protein bands were visualized by color reaction using nitro-blue tetrazolium/5-bromo-4-chloro-3'-indolylphosphate p-toluidine (FUJIFILM Wako Pure Chemical) system. Protein band intensities were determined using Image Studio lite software (LI-COR Biosciences, Lincoln, NB, USA), normalized for amounts of the internal control GAPDH or β -actin and expressed as percentages of values in control cells.

Statistical analysis

Statistical analysis was performed with Graphpad Prism software version 8. Data are presented as means \pm standard error of mean (SEM). Analysis between two groups was done with two-tailed unpaired Student's *t*-test. For comparison between multiple groups, one or two ways ANOVA followed by Bonferroni post hoc test was used

unless stated otherwise. p value < 0.05 was considered to be statistically significant.

Results

Decreased blood pressure in C2 α - and C2 β -double knockout mice

To study the effects of genetic deletion of C2 α and C2 β on blood pressure and vascular smooth muscle contraction, we employed smooth muscle-specific C2 α knockout (C2 α KO) mice, global C2 β -knockout (C2 β ^{-/-} (C2 β KO)) mice, and double knockout (DKO) mice with smooth muscle-specific C2 α KO and global C2 β KO, which we described previously [3, 16]. Smooth muscle-specific C2 α KO mice were generated by mating C2 α ^{fllox/fllox} and SM22 α -Cre transgenic mice. We confirmed that SM22 α promoter-driven Cre expression efficiently deleted the floxed sequence in the R26-tdTomato reporter construct, resulting in the expression of tdTomato protein in aortic smooth muscle layer which also expressed smooth muscle-specific myosin heavy chain isoform Mhc11, but not in the adventitial layer (Fig. 1a). The immunostaining of the aortic sections showed that C2 β was expressed abundantly in the smooth muscle layer and slightly in the endothelium of wild-type mice but not of C2 β KO mice (Fig. 1b). In control C2 α -floxed (C2 α ^{fllox/fllox}) and C2 β KO mice, C2 α was expressed in both the endothelium and smooth muscle layer of the aorta, whereas C2 α expression was deficient in the smooth muscle layer but not the endothelium of smooth muscle-specific C2 α KO mice (Fig. 1c). We performed morphological studies of the aorta and mesenteric artery in DKO and control mice using the immunostaining of the smooth muscle-specific proteins Mhc11 and SM22 α and the endothelial marker CD31 (Fig. 2a, b). The medial smooth muscle and endothelial layers were similar in DKO and control mice, suggesting that the structure of the vasculature was not compromised in DKO mice.

Either C2 α KO mice or C2 β KO mice showed no difference in systolic, diastolic or mean BP compared with control C2 α ^{fllox/fllox} and C2 β ^{+/+} mice, respectively (Fig. 3a, b). In contrast, DKO mice exhibited lower levels of systolic,

diastolic and mean BP compared with control C2 α ^{fllox/fllox} mice (Fig. 3c).

Attenuated contraction of aortic rings and aortic smooth muscle cells from DKO mice

We determined NA- and KCl-induced contractile responses of aortic rings isolated from DKO and control mice. NA-induced dose-dependent contraction was markedly reduced in the aortic rings from DKO mice compared with control mice (Fig. 4a). KCl-induced contraction was also reduced in DKO mice compared with control mice (Fig. 4b).

We next determined contractile responses of MASM isolated from the aortae of control and KO mice. Cells were loaded with Fluo-8 to visualize cell shapes under a fluorescent microscope. The Ca²⁺ ionophore ionomycin (IMC) was employed as a stimulant because MASM lost the responsiveness to KCl-membrane depolarization and receptor agonists including NA, serotonin and a thromboxane analogue during cell culture for isolation. Ionomycin induced marked contraction of MASM from control mice with an increase in cellular Fluo-8 fluorescence (Fig. 5). To quantify cell contraction, a reduction of the planar cell surface area was determined in each cell. C2 α KO cells and C2 β KO cells exhibited the similar extent of IMC-induced contraction compared with each control group of cells (Fig. 5a, b). In contrast, DKO cells showed markedly reduced contraction compared with control MASMs (Fig. 5c). These findings indicate that either C2 α or C2 β is required for contraction, i.e., C2 α and C2 β are engaged in contraction of MASM in a redundant manner.

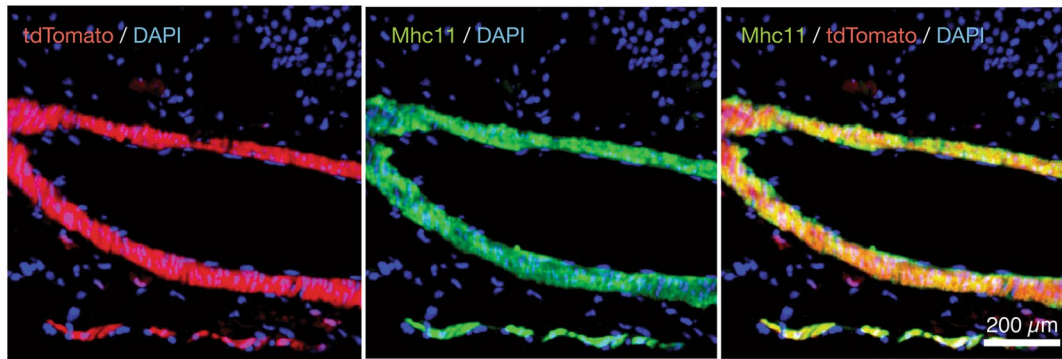
Attenuated contraction of HASM deficient in both C2 α and C2 β

Because MASM were not suitable for further studies of C2 α and C2 β actions due to limited yield of cells isolated by the enzymatic dispersion method, we took advantage of HASMs which were depleted of C2 α and C2 β by transfection of the specific siRNAs. Both C2 α - and C2 β -specific siRNAs effectively and specifically depleted the expression of respective proteins by 75–80% (Fig. 6a).

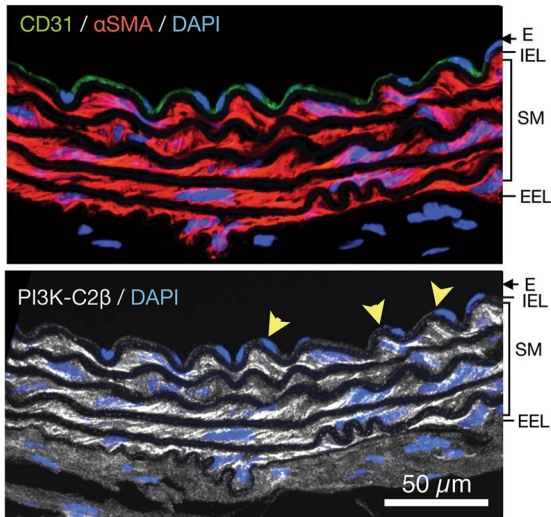
(See figure on next page.)

Fig. 1 Deletion of C2 α and C2 β in the aortic smooth muscle layer of knockout mice. **a** The expression of tdTomato and immunofluorescence staining of myosin heavy chain 11 (Mhc11) in the medial smooth muscle layer of the aorta in SM22 α -Cre; R26-tdTomato reporter mice. Mhc11-positive cells express tdTomato protein. **b** Deletion of C2 β in the medial smooth muscle layer and the endothelium of the aorta in C2 α ^{fllox/fllox} C2 β ^{-/-}; SM22 α -Cre mouse. The sections of the aortic wall were immunostained using anti-C2 β , anti-CD31 and anti- α SMA antibodies. The medial smooth muscle layer (SM) and the endothelium (E) were completely devoid of C2 β expression in C2 α ^{fllox/fllox} C2 β ^{-/-}; SM22 α -Cre mouse (lower right), differently from wild type (BL6) mouse (lower left). IEL internal elastic lamina, EEL external elastic lamina. **c** Marked reduction of C2 α expression in the SM but not the E of the aorta in C2 α ^{fllox/fllox} C2 β ^{-/-}; SM22 α -Cre mouse. The sections of the aortic wall were immunostained using anti-C2 α , anti-CD31 and anti- α SMA antibodies. In **b** and **c**, yellow arrowheads indicate endothelial deletion of C2 β in C2 α ^{fllox/fllox} C2 β ^{-/-} mouse but not of C2 α in C2 α ^{fllox/fllox} C2 β ^{-/-}; SM22 α -Cre mouse, respectively. In **a–c**, nuclei were stained with DAPI

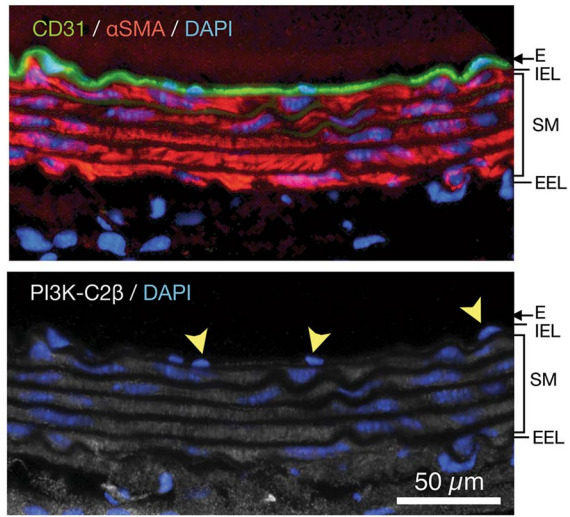
a SM22 α -Cre ; R26-tdTomato aorta



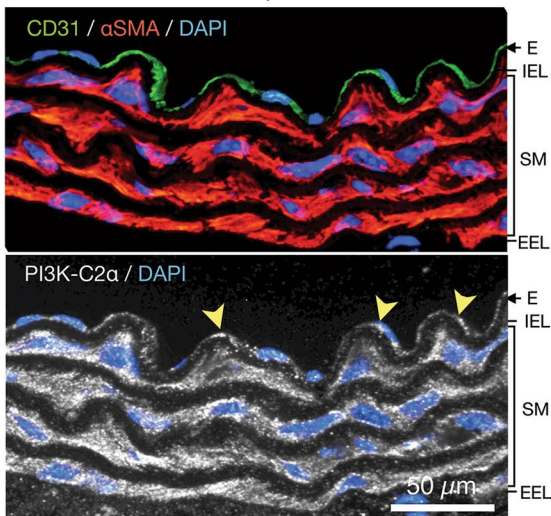
b Wild-type (BL6) aorta



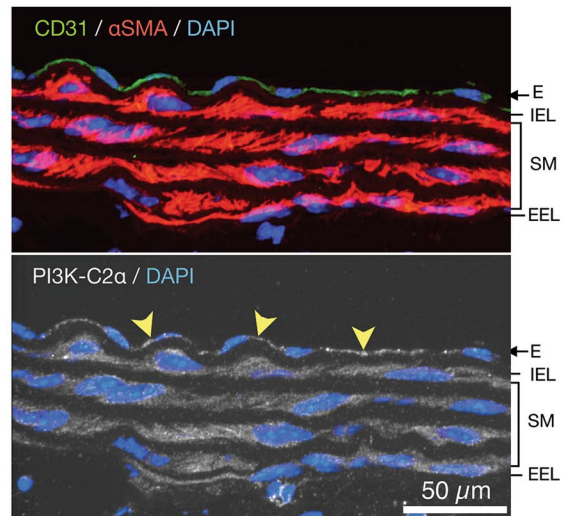
C2 $\alpha^{flox/flox}$; C2 $\beta^{-/-}$; SM22 α -Cre aorta



c C2 $\alpha^{flox/flox}$; C2 $\beta^{-/-}$ aorta



C2 $\alpha^{flox/flox}$; C2 $\beta^{-/-}$; SM22 α -Cre aorta



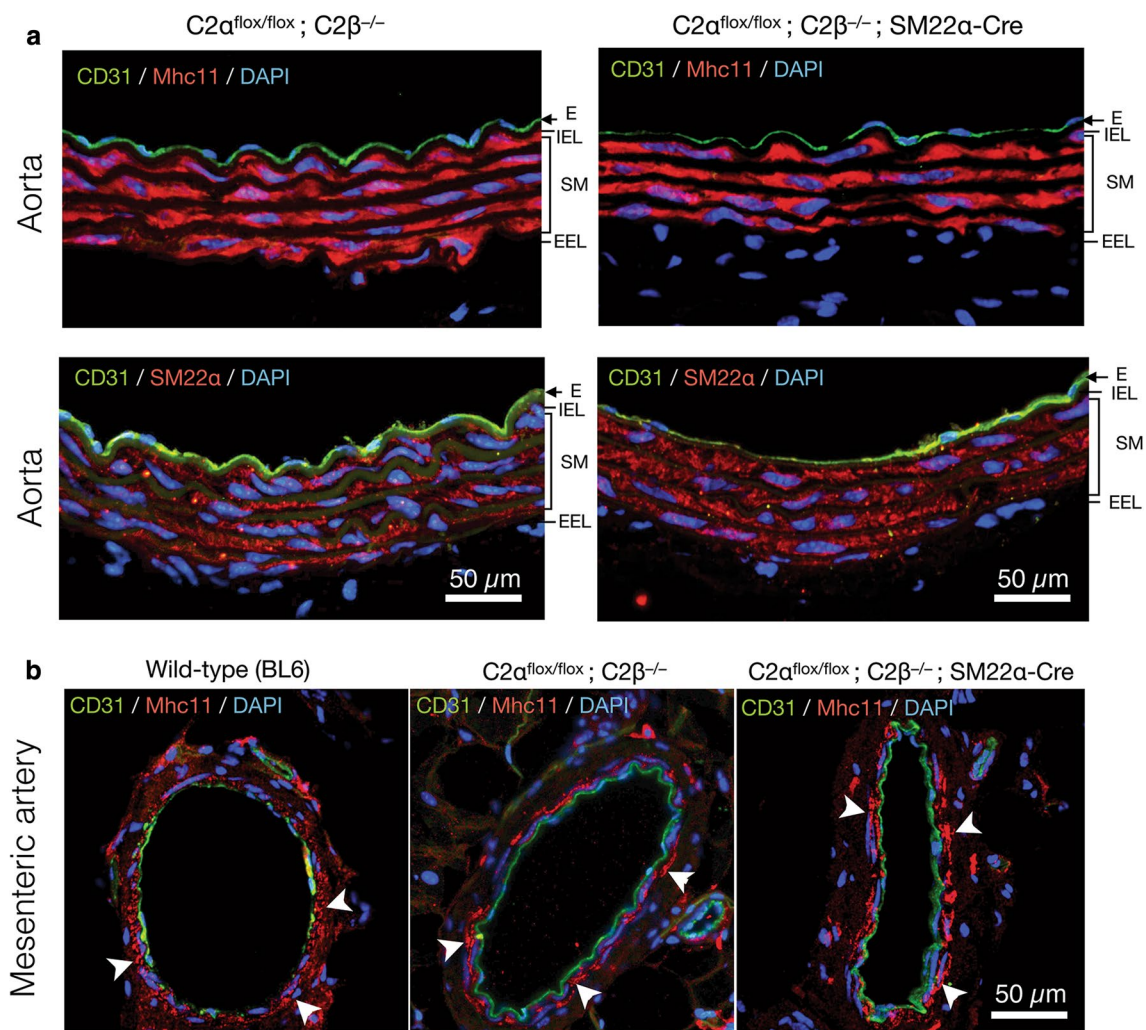


Fig. 2 Expression of the smooth muscle-specific proteins in the aorta and mesenteric artery of control and knockout mice. **a** Immunofluorescence staining of the smooth muscle-specific proteins Mhc11 and SM22 α in the aorta of control ($C2\alpha^{flox/flox}; C2\beta^{-/-}$) and DKO ($C2\alpha^{flox/flox}; C2\beta^{-/-}; SM22\alpha-Cre$) mice. The SM layer was similarly stained by anti-Mhc11 and anti-SM22 α antibodies. **b** Immunofluorescent staining of Mhc11 in the mesenteric artery of wild-type (BL6) (left), $C2\alpha^{flox/flox}; C2\beta^{-/-}$ (middle), and $C2\alpha^{flox/flox}; C2\beta^{-/-}; SM22\alpha-Cre$ mice (right). White arrowheads indicate similar expression of Mhc11 in the SM. In **a** and **b**, nuclei were stained with DAPI

The combination of $C2\alpha$ - and $C2\beta$ -specific siRNAs efficiently inhibited the expression of both $C2\alpha$ and $C2\beta$. Control siRNA-transfected HASM contracted robustly in response to IMC (Fig. 6b and Additional file 1: Video S1). Either singly $C2\alpha$ - or $C2\beta$ -depleted cells showed the similar extents of contraction compared with control HASM (Additional file 2: Video S2 and Additional file 3: Video S3). In contrast, $C2\alpha$ - or $C2\beta$ -doubly depleted HASM showed substantial attenuation of contraction compared with control and single $C2\alpha$ - or $C2\beta$ -depleted cells (Additional file 4: Video S4). Thus, either $C2\alpha$ or $C2\beta$ is required for full contraction of HASM similarly to the responses of mouse aortic rings and MASM

and, therefore, depletion of both $C2\alpha$ and $C2\beta$ severely impairs contraction.

Attenuated phosphorylation of MLC_{20} and MYPT1 in HASMs deficient in both $C2\alpha$ and $C2\beta$

We explored the intracellular mechanisms for the diminished contraction of $C2\alpha$ - and $C2\beta$ -depleted HASM. Single depletion of $C2\alpha$ or $C2\beta$ or double depletion of both $C2\alpha$ and $C2\beta$ did not affect IMC-induced increases in the intracellular free Ca^{2+} concentration ($[Ca^{2+}]_i$) as determined with Fluo-8 as Ca^{2+} indicator (Fig. 6c). Depletion of $C2\alpha$ and $C2\beta$ did not affect the protein expression of smooth muscle-specific myosin heavy chain isoform

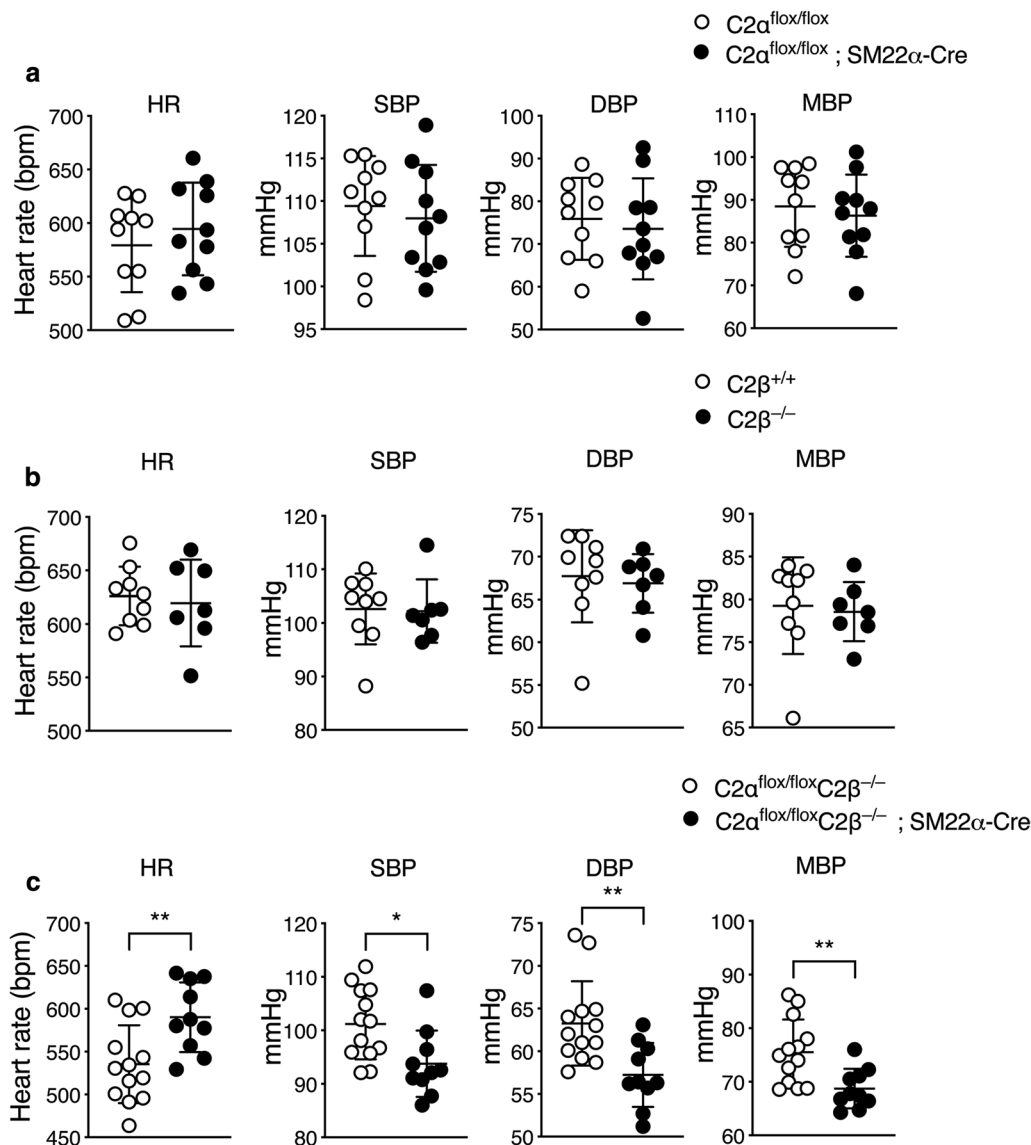


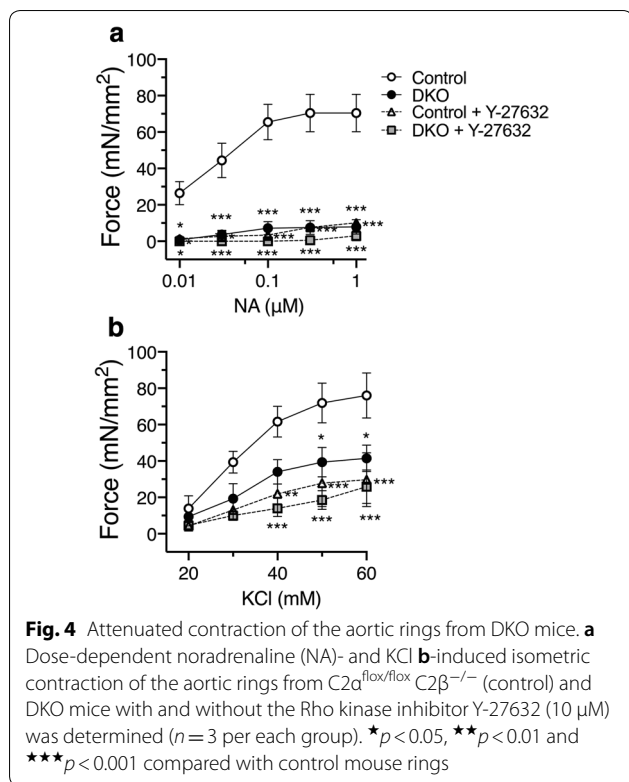
Fig. 3 Blood pressure is decreased in DKO mice. Heart rate (HR), systolic (SBP), diastolic (DBP) and mean (MBP) blood pressure in $C2\alpha^{flox/flox}$ ($n = 10$) and $C2\alpha^{flox/flox}; SM22\alpha-Cre$ mice ($n = 10$) (a), in wild-type ($C2\beta^{+/+}$) ($n = 10$) and $C2\beta^{-/-}$ ($n = 9$) mice (b), and in $C2\alpha^{flox/flox}C2\beta^{-/-}$ ($n = 13$) and $C2\alpha^{flox/flox}C2\beta^{-/-}; SM22\alpha-Cre$ ($n = 10$) mice (c). * $p < 0.05$, ** $p < 0.01$

Mhc11, MLCK or MYPT1, but reduced the expression of MLC_{20} and αSMA in HASM (Fig. 7a). IMC induced time-dependent increases in mono (Ser¹⁹)- and di (Thr¹⁸, and Ser¹⁹)-phosphorylation of MLC_{20} in HASM (Fig. 7b). Double knockdown of $C2\alpha$ and $C2\beta$ substantially reduced mono- and di-phosphorylation of MLC_{20} when evaluated as values corrected for total amount of MLC_{20} . IMC also increased phosphorylation of MYPT1 (Fig. 7c), suggesting that IMC suppressed MLCP activity. Moreover, the Rho kinase inhibitor Y27632 substantially inhibited not only IMC-induced contraction (Fig. 6b), but also

mono- and di-phosphorylation of MLC_{20} and MYPT1 phosphorylation in HASM (Fig. 7c), suggesting that Rho kinase was involved in IMC-induced MLCP inhibition, MLC_{20} phosphorylation and contraction.

Subcellular localization of $C2\alpha$ and $C2\beta$ in HASM

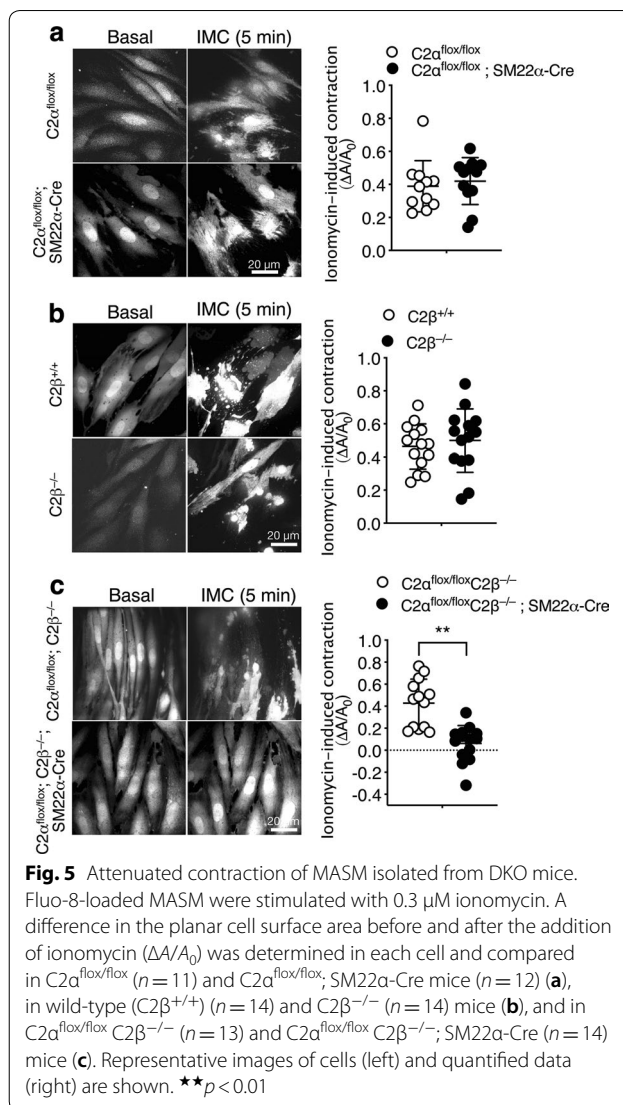
To try to understand the role of $C2\alpha$ and $C2\beta$ in the contractile signaling in more depth, we studied the subcellular localization of $C2\alpha$ and $C2\beta$ in HASMs. We co-transfected HASMs with GFP-tagged $C2\alpha$ (GFP- $C2\alpha$) and mCherry-tagged $C2\beta$ (mCherry- $C2\beta$) and observed



cells by confocal microscopy coupled with super-resolution radial fluctuation (SRRF-Stream) mode. We found that GFP-C2 α was distributed diffusely as fine puncta and as coarse puncta locally in the perinuclear region with some signals at or near the plasma membrane in HASMs (Fig. 8a, upper left and lower views). mCherry-C2 β was distributed in a fibrillary pattern in the peripheral cytoplasmic region close to the plasma membrane and in perinuclear coarse puncta with some co-localization with GFP-C2 α (Fig. 8a, upper right and lower views). In the perinuclear coarse puncta and the peripheral fibrillary localization, mCherry-C2 β was co-localized with GFP-C2 α (Fig. 8a, upper right and lower right view). The subcellular distribution of GFP-C2 α and mCherry-C2 β was similar to that in human umbilical vein endothelial cells [5]. We previously observed the close co-localization of GFP-C2 α and clathrin in human endothelial cells [5]. We found the similar co-localization of GFP-C2 α and clathrin in HASMs (Fig. 8b). mCherry-C2 β was also co-localized with clathrin, but less frequently compared with GFP-C2 α . This finding was also similar to that in human endothelial cells.

Attenuated Rho activation in HASM deficient in both C2 α and C2 β

We determined IMC-induced Rho activation in HASMs, using a FRET imaging technique. Both



IMC- and ET-1-induced Rho activation detectable within 1 min mainly in the intracellular compartment in control HASMs, and it persisted for at least 10 min of the observation time period (Fig. 9a, b, and Additional file 5: Video S5 and Additional file 6: Video S6). In contrast, in cells deficient in both C2 α and C2 β , IMC- and ET-1-induced Rho activation was markedly inhibited with only slight activation observed in the intracellular compartment at 5 to 10 min (Fig. 9a, b, and Additional file 5: Video S5 and Additional file 6: Video S6). In control cells, Rho-FRET signals were partially co-localized with the early endosome marker Rab5. In cells deficient in both C2 α and C2 β , FRET signals were greatly attenuated in both Rab5-positive and negative intracellular sites (Fig. 9c). These observations suggested that C2 α and C2 β were involved in Rho activation in the intracellular compartment.

Discussion

In this study, we demonstrated that class II PI3K C2 α and C2 β have the essential redundant role in the blood pressure regulation and vascular smooth muscle contraction. Mice that have both smooth muscle-specific C2 α deletion and global C2 β deletion are not lethal and therefore allowed us to evaluate the role of C2 α and C2 β in blood pressure regulation. Double KO of C2 α and C2 β but no single KO of either gene resulted in a decrease in arterial blood pressure, indicating that at least one isoform of C2 α and C2 β is necessary for the maintenance of blood pressure. The diminished contractile capacity of vascular smooth muscle from DKO mice suggested that attenuated vascular smooth muscle contraction was involved in hypotension in DKO mice. Moreover, the attenuation of Rho activation and resultant Rho kinase-dependent MLCP inhibition, but not of Ca²⁺ mobilization, was suggested to underlie attenuated vascular contraction and decreased blood pressure in DKO mice. These findings, together with our recent observations of the essential redundant role of C2 α and C2 β in uterine smooth muscle contraction and parturition [17], point to the importance of C2 α and C2 β for activation of Rho and Rho kinase pathway in smooth muscle contraction in mice.

Vascular smooth muscle tone is a major determinant of the blood pressure and directly regulated by the contraction and relaxation state of vascular smooth muscle, which are under the control of various vasoconstrictors and vasodilators, sympathetic nerve activity, and mechanical stress [20–22]. The contractile responses of DKO mouse-derived aortic rings to NA and membrane depolarization were substantially reduced compared with aortic rings from control mice. Smooth muscle contraction is mediated by the two major signaling pathways of Ca²⁺-dependent MLCK activation (Ca²⁺-MLCK pathway) and Rho- and Rho kinase-dependent MLCP inhibition (Rho-MLCP pathway) [23–26]. The increase in the [Ca²⁺]_i activates Ca²⁺/calmodulin-dependent MLCK, leading to MLC₂₀ phosphorylation, and Rho activates its effector Rho kinase, resulting in inhibition of MLCP by phosphorylating the myosin-targeting subunit MYPT1 of MLCP. Rho-MLCP pathway as well as Ca²⁺-MLCK pathway coordinately and effectively increase MLC₂₀

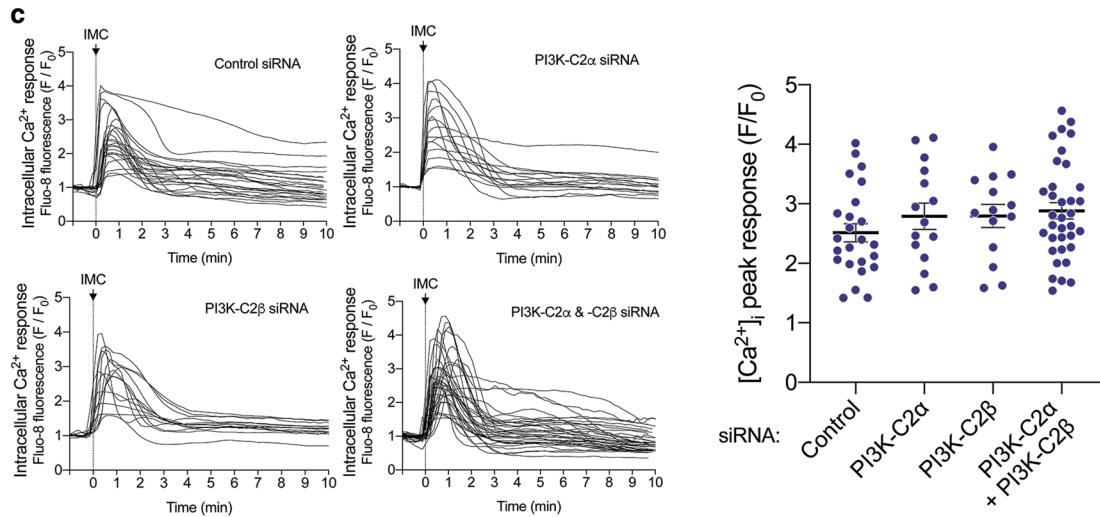
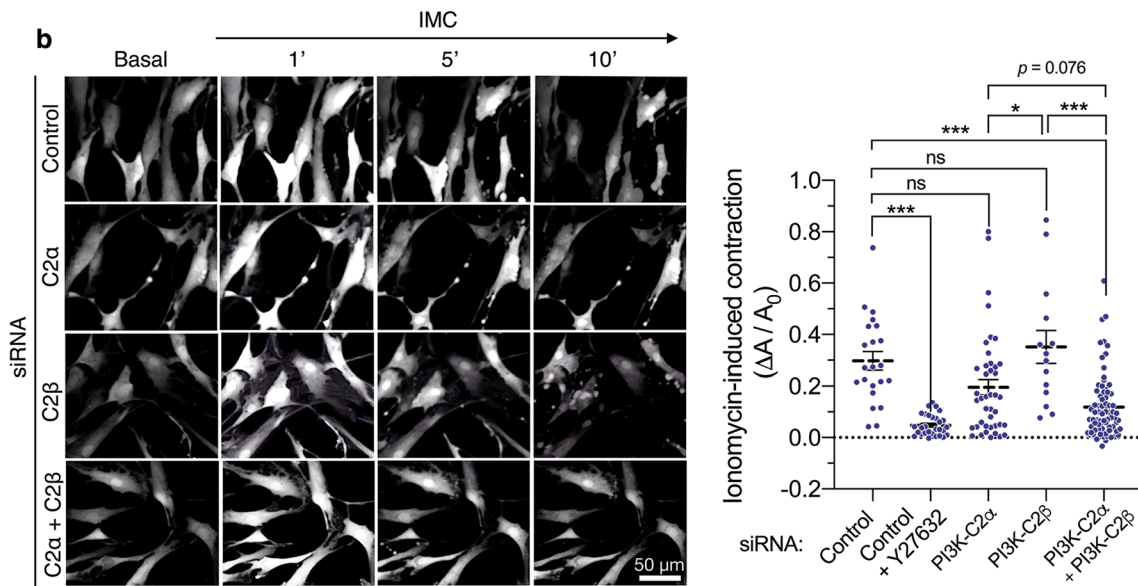
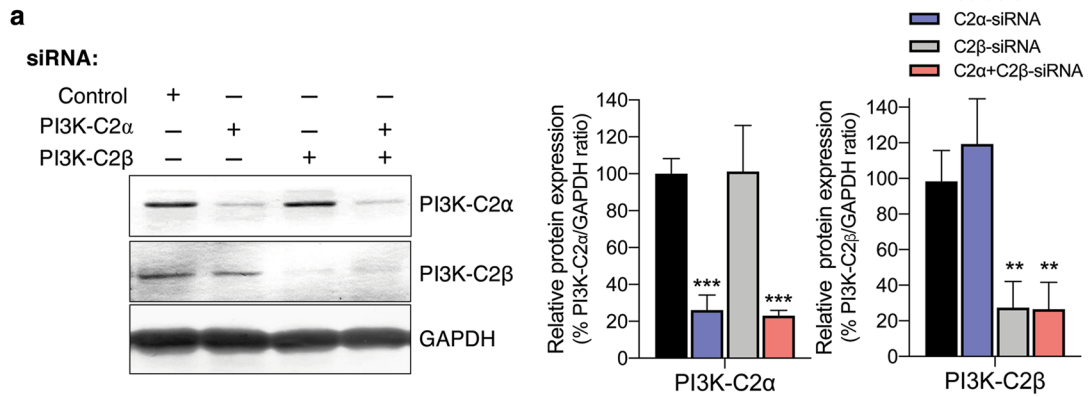
phosphorylation, thus playing a critical role in contraction induced by various agonists including NA, endothelin-1 and thromboxane A₂. We and others previously showed that an increase in [Ca²⁺]_i induced by membrane depolarization and a Ca²⁺ ionophore also resulted in the activation of Rho-MLCP pathway in smooth muscle [27, 28]. In C2 α - and C2 β -dually deficient vascular smooth muscle cells, the activity of Rho pathway but not Ca²⁺ pathway was attenuated compared with control cells, as evaluated with the FRET imaging of Rho activation and phosphorylation status of MYPT1. Therefore, it is likely that the attenuation of Rho signaling resulted in a higher MLCP activity, leading to reductions of MLC₂₀ phosphorylation and contraction in C2 α - and C2 β -deficient vascular smooth muscle cells compared with control cells. We observed the reduced expression of MLC₂₀ and α SMA in HASM with either C2 β single deficiency or C2 α /C2 β double deficiency. It is unknown how C2 β and C2 α /C2 β deficiency resulted in the downregulation of the smooth muscle-specific proteins and remains to be clarified. However, it is unlikely that the reduced expression of MLC₂₀ and α SMA could be involved in the attenuation of contraction because single C2 β depletion failed to inhibit contraction despite the reductions of MLC₂₀ and α SMA expression.

We found in the present study that the Ca²⁺-ionophore ionomycin and endothelin-1-induced vigorous Rho activation mainly in the intracellular compartment of vascular smooth muscle cells. The intracellular localization of Rho activation site was consistent with our previous observations in mouse uterine smooth muscle cells [17] and human vascular endothelial cells [3], and reports by others in other types of cells [29–32]. Our study suggested that at least a part of the Rho activation sites was Rab5-positive structures, i.e., early endosomes.

The present study clearly showed that C2 α and C2 β were required for Rho activation in the intracellular compartment in vascular smooth muscle cells. How are C2 α and C2 β engaged in Rho activation at the early endosomes and other intracellular structures? Previous studies [3, 30–32] showed that C2 α is preferentially localized to clathrin-coated pits and vesicles and plays an indispensable role in clathrin-dependent endocytosis.

(See figure on next page.)

Fig. 6 Attenuated contraction of C2 α - and C2 β -depleted HASM. **a** Knockdown of C2 α and C2 β proteins in HASM by the specific siRNAs. HASMs were transfected with control-, C2 α - and C2 β -siRNAs and subjected to Western blot analyses for C2 α and C2 β protein expression. Left, Western blotting. Middle and right panels, quantified data of C2 α and C2 β protein expression. **b** Attenuated contraction of C2 α - and C2 β -double depleted HASM. IMC (0.3 μ M)-induced contraction was determined as in Fig. 5. A portion of control siRNA-transfected HASM were pretreated or unpretreated with Y-27632 (10 μ M) for 5 min and stimulated with ionomycin for 10 min. Representative images of cells (left) and quantified data (right) are shown. * p < 0.05 and *** p < 0.001 in the indicated comparisons. **c** No difference in ionomycin-induced increases in the [Ca²⁺]_i in HASM transfected with control-, C2 α - and C2 β -siRNAs. Left, time-dependent changes in the [Ca²⁺]_i in ionomycin-stimulated cells. Right, quantified data of the peak response of the [Ca²⁺]_i



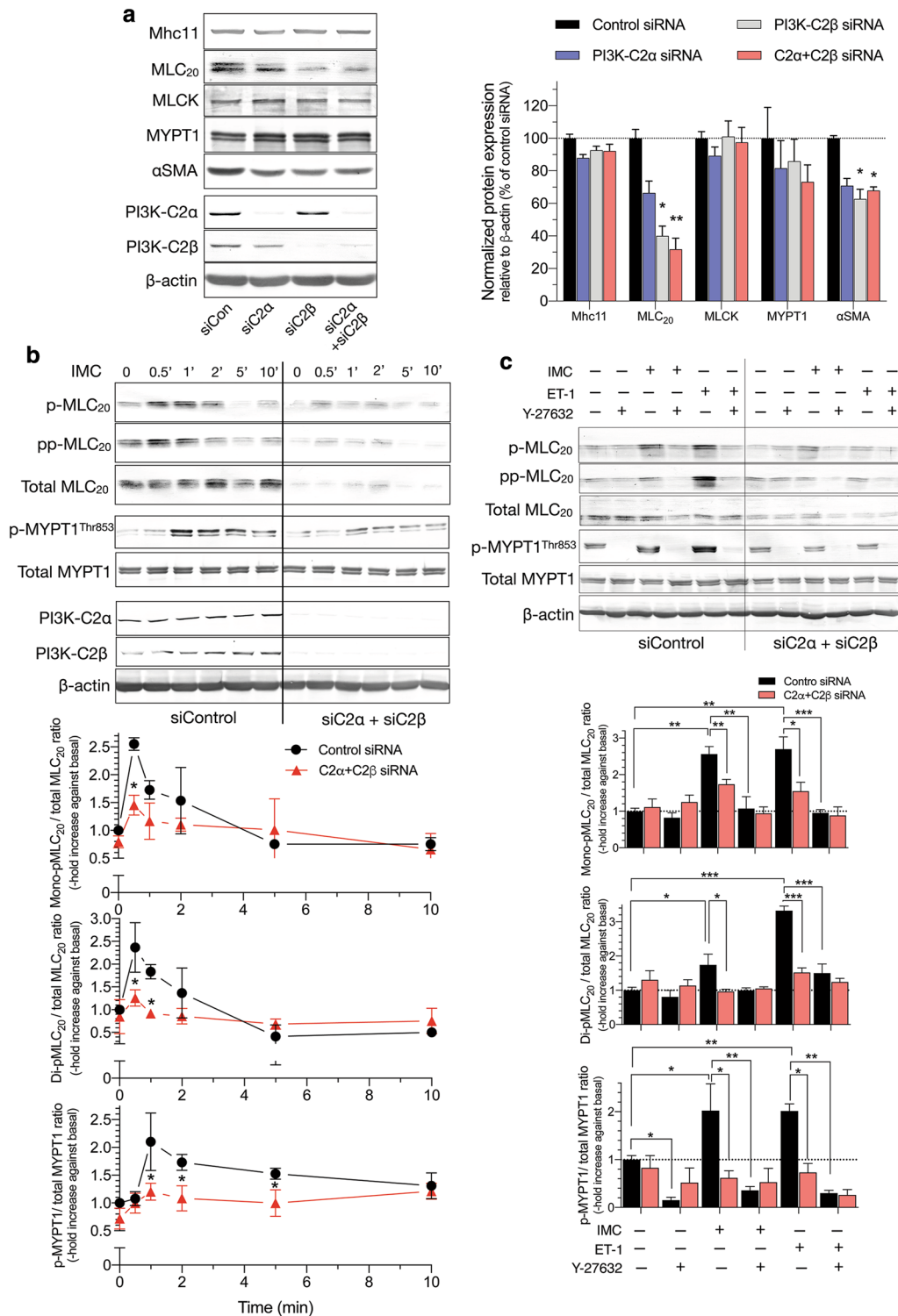
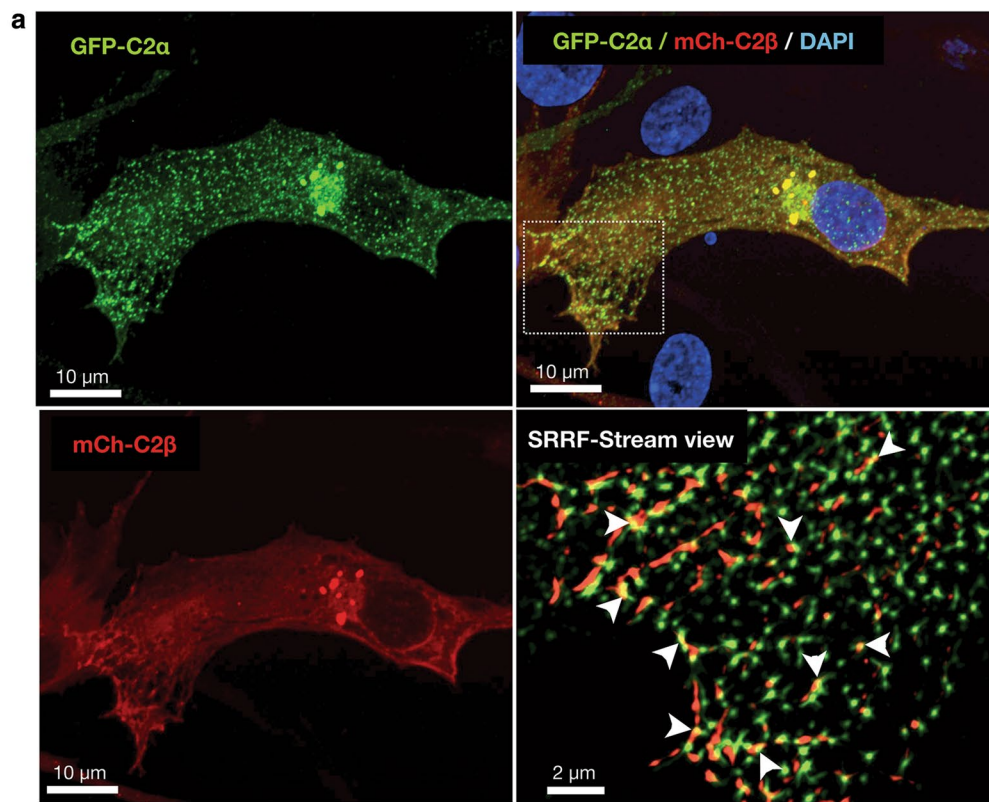


Fig. 7 Attenuated phosphorylation of MLC₂₀ and MYPT1 in C2α- and C2β-depleted HASM. **a** Effects of C2α and C2β knockdown on the expression of smooth muscle-specific proteins in HASM. Cells were transfected with control-, C2α- and C2β-siRNAs and subjected to Western blot analyses. Left, Western blots. Middle and right panels, quantified data of Mhc11, MLC₂₀, MLCK, MYPT1 and αSMA. **b** Attenuated mono- and di-phosphorylation of MLC₂₀ and phosphorylation of MYPT1 in C2α- and C2β-double depleted HASM. HASM were transfected with control-, C2α- and C2β-siRNAs and stimulated with 0.3 μM ionomycin for 10 min. **p* < 0.05 compared with control siRNA-transfected cells. **c** Effects of ROCK inhibitor Y-27632 on mono- and di-phosphorylation of MLC₂₀ and phosphorylation of MYPT1 in C2α- and C2β-double depleted HASM. **p* < 0.05, ***p* < 0.01 and ****p* < 0.001 in the indicated comparisons



b

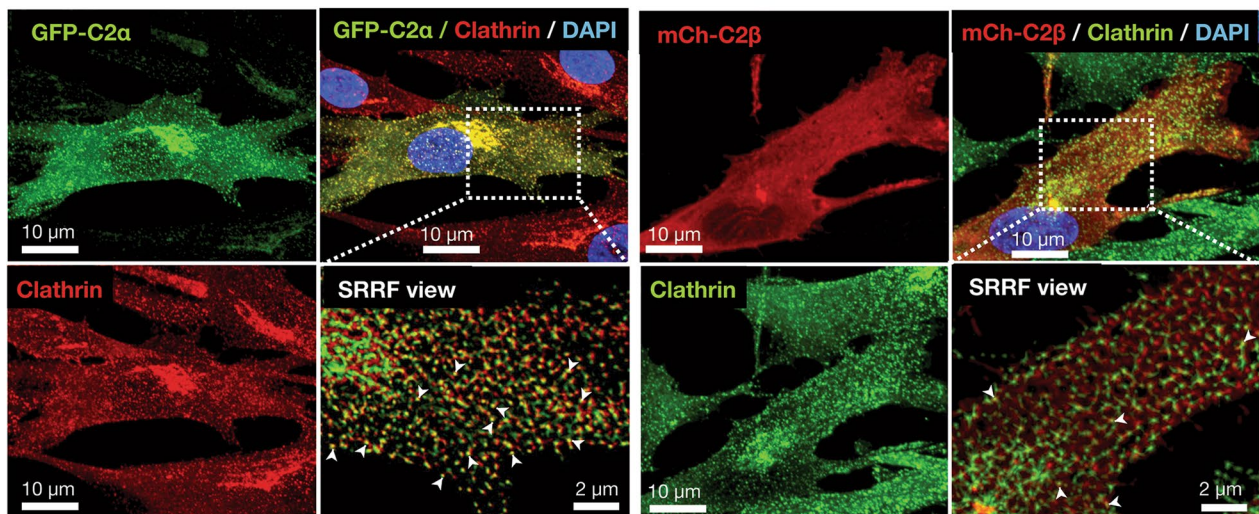


Fig. 8 Subcellular distribution of C2 α and C2 β in HASM. **a** Confocal images of subcellular distribution of GFP-C2 α and mCherry-C2 β . Cells were co-transfected with the expression vectors for GFP-C2 α and mCherry-C2 β . GFP-C2 α is distributed at diffuse fine puncta and perinuclear coarse puncta. mCherry-C2 β (mCh-C2 β) is distributed at perinuclear coarse puncta and plasma membrane. mCherry-C2 β is also distributed diffusely in the mesh-like pattern with some co-localization with GFP-C2 α (arrowheads in the lower right panel). **b** Co-localization of GFP-C2 α and mCherry-C2 β with clathrin. Cells were co-transfected with the expression vectors of GFP-C2 α and mCherry-C2 β , and subjected to anti-clathrin heavy chain immunofluorescence staining. Nuclei were stained with DAPI. PI3K-C2 α and PI3K-C2 β were co-localized with clathrin heavy chain diffusely and at the perinuclear region although the co-localization of PI3K-C2 β and clathrin heavy chain was less frequent

C2 α mainly produces PI(3,4)P₂ [33–37] and recruits PI(3,4)P₂-binding domain-possessing proteins including SNX9, thus facilitating growth and maturation of clathrin-coated pits and their conversion into clathrin-coated vesicles. A functional role and intracellular localization of C2 β was poorly understood compared with C2 α . We recently demonstrated that C2 β was localized at the focal filamentous actin (actin patches) in the peripheral cytoplasmic regions and clathrin-coated pits and vesicles in vascular endothelial cells and that C2 β as well as C2 α were necessary for clathrin-dependent fluid-phase endocytosis [5]. The present study showed that vascular smooth muscle cells exhibited the similar intracellular distribution of C2 β to that in endothelial cells. Activation of Rho is mediated by a guanine nucleotide-exchange factor (GEF) [38]. Therefore, a GEF is likely recruited to early endosomes and other intracellular structures in stimulated vascular smooth muscle cells. In the case of ET-1-stimulated vascular smooth muscle cells, it could be possible that class II PI3K might be necessary for the endocytosis of ET-1-bound receptor into the early endosomes and that the endocytosed receptor, in turn, might recruit a GEF via the heterotrimeric G protein G_{12/13} to result in Rho activation. When vascular smooth muscle cells are stimulated with IMC, a Ca²⁺-induced Rho activation mechanism operates [12, 27]. The Ca²⁺-induced Rho activation may be mediated by a particular type of GEF and the recruitment of the particular GEF may require a process of endocytosis of the GEF molecule itself or a regulatory molecule of the GEF [39]. These endocytic processes may be dependent on PI3K-C2 α and PI3K-C2 β . Further studies are required for defining the exact role of C2 α and C2 β in the intracellular Rho activation.

Our previous studies showed that siRNA-mediated specific knockdown of only C2 α -inhibited contraction of vascular smooth muscle cells derived from rat aortae [12, 13]. In contrast, the present study showed that knockdown of C2 α alone was not enough to completely inhibit contraction of mouse and human vascular smooth muscle cells, which may suggest that C2 β can compensate for

a defect caused by C2 α deficiency in mouse and human vascular smooth muscle cells; C2 β may be able to compensate for insufficient PI(3,4)P₂ production due to C2 α depletion in clathrin-coated pits and vesicles and other intracellular sites in mouse and human, but not rat, vascular smooth muscle cells. It is unknown at present whether the expression levels of C2 β or differences in the subcellular localization of C2 β could bring about the species difference in C2 α - and C2 β -dependence of vascular smooth muscle contraction. The exact molecular mechanisms for the species-specific dependence on C2 α and C2 β of vascular smooth muscle contraction remain to be clarified.

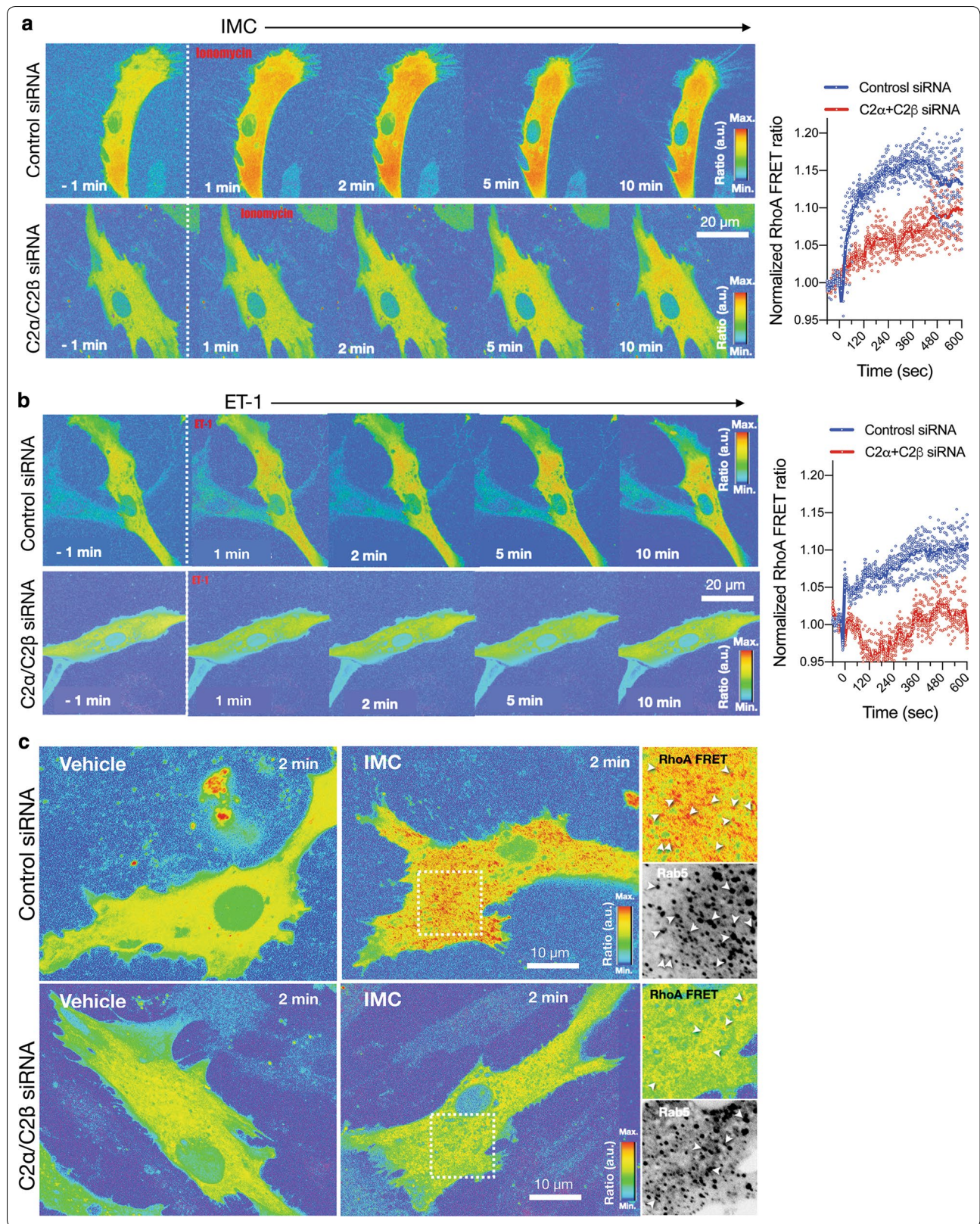
Because the RhoA–Rho kinase–MLCP pathway is one of the major contractile mechanism in vascular smooth muscle contraction [23, 24, 26], the novel role of C2 α and C2 β in Rho–Rho kinase–MLCP pathway may provide some insight about understanding the pathophysiology and development of new therapies for cardiovascular diseases including hypertension and vasospasms. For example, a class II PI3K inhibitor, which inhibits Rho activation and thereby stimulates MLCP in vascular smooth muscle, may be a candidate for developing new anti-hypertensive and spasmolytic agents. Better understanding of the C2 α and C2 β actions at the cellular and molecular levels is required to unravel the pathophysiological role of human class II PI3K.

Conclusions

The present study showed the importance of C2 α and C2 β in the regulation of the Rho–Rho kinase–MLCP pathway and contraction in vascular smooth muscle and blood pressure regulation. C2 α and C2 β are required for Ca²⁺- and receptor agonist-elicited Rho activation in the intracellular compartment. The role of C2 α and C2 β is essential for vascular smooth muscle contraction, but compensatory for deficiency of each other. Further study is required to reveal the exact mechanism of C2 α - and C2 β -dependent Rho activation in vascular smooth muscle.

(See figure on next page.)

Fig. 9 FRET imaging of attenuated Rho activation in C2 α - and C2 β -depleted HASM. **a** Effects of C2 α and C2 β knockdown on the expression of IMC (0.3 μ M)-induced Rho activation as evaluated with FRET imaging in control and C2 α - and C2 β -double depleted HASM. Left, representative images. Right, quantified data of time-dependent Rho-FRET signals. **b** Effects of C2 α and C2 β knockdown on ET-1 (1 μ M)-induced Rho activation as evaluated with FRET imaging in control and C2 α - and C2 β -double depleted HASM. Left, representative images. Right, quantified data of time-dependent Rho-FRET signals. **c** Partial co-localization of RhoA-FRET signals with the early endosome marker Rab5. Cells were transfected with BFP-Rab5 expression vector and the co-localization of RhoA-FRET signals and BFP-Rab5 was determined



Supplementary information

Supplementary information accompanies this paper at <https://doi.org/10.1186/s12576-020-00745-2>.

Additional file 1: Video S1. The time-lapse imaging of ionomycin-induced $[Ca^{2+}]_i$ response and contraction of control siRNA-transfected HASM. Control siRNA-transfected, the fluorescent Ca^{2+} indicator fluo-8 loaded HASM cells were stimulated with ionomycin (0.3 μ M) at 1 min, and contractile responses and changes in $[Ca^{2+}]_i$ response were continuously monitored for 10 min (10-s intervals).

Additional file 2: Video S2. The time-lapse imaging of ionomycin-induced $[Ca^{2+}]_i$ response and contraction of PI3K-C2 α siRNA-transfected HASM. PI3K-C2 α specific siRNA-transfected, the fluorescent Ca^{2+} indicator fluo-8 loaded HASM cells were stimulated with ionomycin (0.3 μ M) at 1 min, and contractile responses and changes in $[Ca^{2+}]_i$ response were continuously monitored for 10 min (10-s intervals).

Additional file 3: Video S3. The time-lapse imaging of ionomycin-induced $[Ca^{2+}]_i$ response and contraction of PI3K-C2 β siRNA-transfected HASM. PI3K-C2 β specific siRNA-transfected, the fluorescent Ca^{2+} indicator fluo-8 loaded HASM cells were stimulated with ionomycin (0.3 μ M) at 1 min, and contractile responses and changes in $[Ca^{2+}]_i$ response were continuously monitored for 10 min (10-s intervals).

Additional file 4: Video S4. The time-lapse imaging of ionomycin-induced $[Ca^{2+}]_i$ response and contraction of PI3K-C2 α and -C2 β siRNA-transfected HASM. PI3K-C2 α and -C2 β specific siRNA-transfected, the fluorescent Ca^{2+} indicator fluo-8 loaded HASM cells were stimulated with ionomycin (0.3 μ M) at 1 min, and contractile responses and changes in $[Ca^{2+}]_i$ response were continuously monitored for 10 min (10-s intervals).

Additional file 5: Video S5. The time-lapse imaging of RhoA-FRET in ionomycin-stimulated HASM. HASM cells were transfected with RhoA-FRET probe expression vector and either control siRNA (left) or PI3K-C2 α and -C2 β specific siRNAs (right), and stimulated with ionomycin (0.3 μ M) at 1 min. RhoA-FRET signals were monitored by confocal microscopy for 10 min (10 s-intervals). Note that the addition of ionomycin resulted in rapid activation of RhoA in control cells whereas ionomycin-induced RhoA activation was substantially reduced in C2 α - and C2 β -depleted cells.

Additional file 6: Video S6. The time-lapse imaging of RhoA-FRET in ET-1-stimulated HASM. HASM cells were transfected with RhoA-FRET probe expression vector and either control siRNA (left) or PI3K-C2 α - and -C2 β specific siRNAs (right), and stimulated with endothelin-1 (1 μ M) at 1 min. RhoA-FRET signals were monitored by confocal microscopy for 10 min (10 s-intervals). Note that endothelin-1 resulted in rapid activation of RhoA in control cells whereas endothelin-1-induced RhoA activation was substantially reduced in C2 α - and C2 β -depleted cells.

Abbreviations

PI3K: Phosphoinositide 3-kinases; C2 α : Phosphoinositide 3-kinase-C2 α ; C2 β : Phosphoinositide 3-kinase-C2 β ; $[Ca^{2+}]_i$: Intracellular free Ca^{2+} concentration; Cre: Cre recombinase; R26-tdTomato: Rosa26-CAG-loxP-stop-loxP-tdTomato; DAPI: 4',6-Diamidino-2-phenylindole; KO: Knockout; DKO: Double knockout; FRET: Fluorescence resonance energy transfer; GEF: Guanine nucleotide exchange factor; HBSS: Hanks' balanced salt solution; MLC₂₀: 20-kDa myosin light chain; MLCK: Myosin light chain kinase; MLCP: Myosin light chain phosphatase; IMC: Ionomycin; ET-1: Endothelin-1; NA: Noradrenaline; PI(3,4,5)₂: Phosphatidylinositol 3,4-bisphosphate; SRRF: Super-resolution radial fluctuation; VEGF: Vascular endothelial growth factor; GFP: Green fluorescent protein; MASM: Mouse aortic smooth muscle cells; HASM: Human aortic smooth muscle cells; α SMA: α -Smooth muscle actin; BP: Blood pressure.

Acknowledgements

We thank Ms. Chiemi Hirose for secretarial assistance, and also thank the members of Department of Physiology for their support and assistance.

Authors' contributions

SI, KY, SA and YT designed the study. SI, KY, SA and HY performed experiments. KI helped experiments. SI, KY, SA and YT analyzed the data. SI, KY, NT and YT wrote the manuscript. All authors read and approved the final manuscript.

Funding

This study was supported by Grants from the Ministry of Education, Culture, Sports, Science and Technology (MEXT) of Japan (25116711 to Y.T.), and the Japan Society for the Promotion of Science (17K08532 to K.Y., 16K18988 to S.A., 16K15409 to K.I., 17K08542 to N.T., 15H04673 to Y.T.). The funders had no role in study design, data collection and analysis, decision to publish, or preparation of the manuscript.

Availability of data and materials

The data that support the findings of this study are available from the corresponding author on reasonable request.

Ethics approval and consent to participate

All mouse experiments were approved by the Committee on Animal Experimentation of Kanazawa University.

Consent for publication

Not applicable.

Competing interests

The authors declare that they have no conflict of interest.

Author details

¹ Department of Physiology, Kanazawa University Graduate School of Medical Sciences, 13-1 Takara-machi, Kanazawa, Ishikawa 920-8640, Japan. ² Department of Health Science, Ishikawa Prefectural University, Kahoku, Ishikawa 929-1210, Japan.

Received: 22 January 2020 Accepted: 10 March 2020

Published online: 19 March 2020

References

- Janku F, Yap TA, Meric-Bernstam F (2018) Targeting the PI3K pathway in cancer: are we making headway? *Nat Rev Clin Oncol* 15:273–291. <https://doi.org/10.1038/nrclinonc.2018.28>
- Bilanges B, Posor Y, Vanhaesebroeck B (2019) PI3K isoforms in cell signalling and vesicle trafficking. *Nat Rev Mol Cell Biol* 20:515–534. <https://doi.org/10.1038/s41580-019-0129-z>
- Yoshioka K, Yoshida K, Cui H, Wakayama T, Takuwa N, Okamoto Y, Du W, Qi X, Asanuma K, Sugihara K, Aki S, Miyazawa H, Biswas K, Nagakura C, Ueno M, Iseki S, Schwartz RJ, Okamoto H, Sasaki T, Matsui O, Asano M, Adams RH, Takakura N, Takuwa Y (2012) Endothelial PI3K-C2 α , a class II PI3K, has an essential role in angiogenesis and vascular barrier function. *Nat Med* 18:1560–1569. <https://doi.org/10.1038/nm.2928>
- Gulluni F, De Santis MC, Margaria JP, Martini M, Hirsch E (2019) Class II PI3K functions in cell biology and disease. *Trends Cell Biol* 29:339–359. <https://doi.org/10.1016/j.tcb.2019.01.001>
- Aung KT, Yoshioka K, Aki S, Ishimaru K, Takuwa N, Takuwa Y (2019) The class II phosphoinositide 3-kinases PI3K-C2 α and PI3K-C2 β differentially regulate clathrin-dependent pinocytosis in human vascular endothelial cells. *J Physiol Sci* 69:263–280. <https://doi.org/10.1007/s12576-018-0644-2>
- Marat AL, Haucke V (2016) Phosphatidylinositol 3-phosphates-at the interface between cell signalling and membrane traffic. *EMBO J* 35:561–579. <https://doi.org/10.15252/embj.201593564>
- Wallroth A, Koch PA, Marat AL, Krause E, Haucke V (2019) Protein kinase N controls a lysosomal lipid switch to facilitate nutrient signalling via mTORC1. *Nat Cell Biol* 21:1093–1101. <https://doi.org/10.1038/s41556-019-0377-3>
- Franco I, Gulluni F, Campa CC, Costa C, Margaria JP, Cirraolo E, Martini M, Monteyne D, De Luca E, Germena G, Posor Y, Maffucci T, Marengo S, Haucke V, Falasca M, Perez-Morga D, Boletta A, Merlo GR, Hirsch E (2014) PI3K class II alpha controls spatially restricted endosomal PtdIns3P and Rab11 activation to promote primary cilium function. *Dev Cell* 28:647–658. <https://doi.org/10.1016/j.devcel.2014.01.022>
- Falasca M, Maffucci T (2012) Regulation and cellular functions of class II phosphoinositide 3-kinases. *Biochem J* 443:587–601. <https://doi.org/10.1042/BJ20120008>
- Domin J, Pages F, Volinia S, Rittenhouse SE, Zvebil MJ, Stein RC, Waterfield MD (1997) Cloning of a human phosphoinositide 3-kinase with a

- C2 domain that displays reduced sensitivity to the inhibitor wortmannin. *Biochem J* 326:139–147. <https://doi.org/10.1042/bj3260139>
11. Stein RC, Waterfield MD (2000) PI3-kinase inhibition: a target for drug development? *Mol Med Today* 6:347–357. [https://doi.org/10.1016/s1357-4310\(00\)01770-6](https://doi.org/10.1016/s1357-4310(00)01770-6)
 12. Wang Y, Yoshioka K, Azam MA, Takuwa N, Sakurada S, Kayaba Y, Sugimoto N, Inoki I, Kimura T, Kuwaki T, Takuwa Y (2006) Class II phosphoinositide 3-kinase α -isoform regulates Rho, myosin phosphatase and contraction in vascular smooth muscle. *Biochem J* 394:581–592. <https://doi.org/10.1042/BJ20051471>
 13. Yoshioka K, Sugimoto N, Takuwa N, Takuwa Y (2007) Essential role for class II phosphoinositide 3-kinase α -isoform in Ca^{2+} -induced, Rho- and Rho kinase-dependent regulation of myosin phosphatase and contraction in isolated vascular smooth muscle cells. *Mol Pharmacol* 71:912–920. <https://doi.org/10.1124/mol.106.032599>
 14. Azam MA, Yoshioka K, Ohkura S, Takuwa N, Sugimoto N, Sato K, Takuwa Y (2007) Ca^{2+} -independent, inhibitory effects of cyclic adenosine 5'-monophosphate on Ca^{2+} regulation of phosphoinositide 3-kinase C2 α , Rho, and myosin phosphatase in vascular smooth muscle. *J Pharmacol Exp Ther* 320:907–916. <https://doi.org/10.1124/jpet.106.111443>
 15. Seok YM, Azam MA, Okamoto Y, Sato A, Yoshioka K, Maeda M, Kim I, Takuwa Y (2010) Enhanced Ca^{2+} -dependent activation of phosphoinositide 3-kinase class II α isoform-Rho axis in blood vessels of spontaneously hypertensive rats. *Hypertension* 56:934–941. <https://doi.org/10.1161/HYPERTENSIONAHA.110.160853>
 16. Harada K, Truong AB, Cai T, Khavari PA (2005) The class II phosphoinositide 3-kinase C2 β is not essential for epidermal differentiation. *Mol Cell Biol* 25:11122–11130. <https://doi.org/10.1128/MCB.25.24.11122-11130.2005>
 17. Sarker MAK, Aki S, Yoshioka K, Kuno K, Okamoto Y, Ishimaru K, Takuwa N, Takuwa Y (2019) Class II PI3Ks α and β are required for Rho-dependent uterine smooth muscle contraction and parturition in mice. *Endocrinology* 160:235–248. <https://doi.org/10.1210/en.2018-00756>
 18. Cui H, Okamoto Y, Yoshioka K, Du W, Takuwa N, Zhang W, Asano M, Shibamoto T, Takuwa Y (2013) Sphingosine-1-phosphate receptor 2 protects against anaphylactic shock through suppression of endothelial nitric oxide synthase in mice. *J Allergy Clin Immunol* 132:1205–1214. <https://doi.org/10.1016/j.jaci.2013.07.026>
 19. Kitatani K, Usui T, Sriraman SK, Toyoshima M, Ishibashi M, Shigeta S, Nagase S, Sakamoto M, Ogiso H, Okazaki T, Hannun Y (2016) Ceramide limits phosphatidylinositol-3-kinase C2 β -controlled cell motility in ovarian cancer: potential of ceramide as a metastasis-suppressor lipid. *Oncogene* 35:2801–2812. <https://doi.org/10.1038/onc.2015.330>
 20. Wirth A, Wang S, Takefuji M, Tang C, Althoff TF, Schweda F, Wettschureck-Offermanns WNN (2016) Age-dependent blood pressure elevation is due to increased vascular smooth muscle tone mediated by G-protein signaling. *Cardiovasc Res* 109:131–140. <https://doi.org/10.1093/cvr/cvv249>
 21. Mendelsohn ME (2005) In hypertension, the kidney is not always the heart of the matter. *J Clin Invest* 115:840–844. <https://doi.org/10.1172/JCI24806>
 22. Guyenet PG (2006) The sympathetic control of blood pressure. *Nat Rev Neurosci* 7:335–346. <https://doi.org/10.1038/nrn1902>
 23. Sakurada S, Okamoto H, Takuwa N, Sugimoto N, Takuwa Y (2001) Rho activation in excitatory agonist-stimulated vascular smooth muscle. *Am J Physiol Cell Physiol* 281:571–578. <https://doi.org/10.1152/ajpcell.2001.281.2.C571>
 24. Ito M, Nakano T, Erdodi F, Hartshorne DJ (2004) Myosin phosphatase: structure, regulation and function. *Mol Cell Biochem* 259:197–209. <https://doi.org/10.1023/b:mcbi.0000021373.14288.00>
 25. Stull JT, Lin PJ, Krueger JK, Trehwella J, Zhi G (1998) Myosin light chain kinase: functional domains and structural motifs. *Acta Physiol Scand* 164:471–482. <https://doi.org/10.1111/j.1365-201x.1998.tb10699.x>
 26. Somlyo AP, Somlyo AV (2003) Ca^{2+} sensitivity of smooth muscle and nonmuscle myosin II: modulated by G proteins, kinases, and myosin phosphatase. *Physiol Rev* 83:1325–1358. <https://doi.org/10.1152/physrev.00023.2003>
 27. Sakurada S, Takuwa N, Sugimoto N, Wang Y, Seto M, Sasaki Y, Takuwa Y (2003) Ca^{2+} -dependent activation of Rho and Rho kinase in membrane depolarization-induced and receptor stimulation-induced vascular smooth muscle contraction. *Circ Res* 93:548–556. <https://doi.org/10.1161/01.RES.0000090998.08629.60>
 28. Janssen LJ, Tazzeo T, Zuo J, Pertens E, Keshavjee S (2004) KCl evokes contraction of airway smooth muscle via activation of RhoA and Rho-kinase. *Am J Physiol Lung Cell Mol Physiol* 287:L852–L858. <https://doi.org/10.1152/ajplung.00130.2004>
 29. Pertz O, Hodgson L, Klemke RL, Hahn KM (2006) Spatiotemporal dynamics of RhoA activity in migrating cells. *Nature* 440:1069–1072. <https://doi.org/10.1038/nature04665>
 30. Machacek M, Hodgson L, Welch C, Elliott H, Pertz O, Nalbant P, Abell A, Johnson GL, Hahn KM, Danuser G (2009) Coordination of Rho GTPase activities during cell protrusion. *Nature* 461:99–103. <https://doi.org/10.1038/nature08242>
 31. Ngok SP, Geyer R, Liu M, Kourtidis A, Agrawal S, Wu C, Seerapu HR, Lewis-Tuffin LJ, Moodie KL, Huvelde D, Marx R, Baraban JM, Storz P, Horowitz A, Anastasiadis PZ (2012) VEGF and angiopoietin-1 exert opposing effects on cell junctions by regulating the Rho GEF Syx. *J Cell Biol* 199:1103–1115. <https://doi.org/10.1083/jcb.201207009>
 32. Wu C, Horowitz A (2011) Membrane traffic as a coordinator of cell migration and junction remodeling. *Commun Integr Biol* 4:703–705. <https://doi.org/10.4161/cib.17140>
 33. Gaidarov I, Smith ME, Domin J, Keen JH (2001) The class II phosphoinositide 3-kinase C2 α is activated by clathrin and regulates clathrin-mediated membrane trafficking. *Mol Cell* 7:443–449. [https://doi.org/10.1016/s1097-2765\(01\)00191-5](https://doi.org/10.1016/s1097-2765(01)00191-5)
 34. Posor Y, Eichhorn-Gruenig M, Puchkov D, Schoneberg J, Ullrich A, Lampe A, Muller R, Zarbakhsh S, Gulluni F, Hirsch E, Krauss M, Schultz C, Schmorranzer J, Noe F, Haucke V (2013) Spatiotemporal control of endocytosis by phosphatidylinositol-3,4-bisphosphate. *Nature* 499:233–237. <https://doi.org/10.1038/nature12360>
 35. Wallroth A, Haucke V (2018) Phosphoinositide conversion in endocytosis and the endolysosomal system. *J Biol Chem* 293:1526–1535. <https://doi.org/10.1074/jbc.R117.000629>
 36. Aki S, Yoshioka K, Okamoto Y, Takuwa N, Takuwa Y (2015) Phosphatidylinositol 3-kinase class II α -isoform PI3K-C2 α is required for transforming growth factor β -induced smad signaling in endothelial cells. *J Biol Chem* 290:6086–6105. <https://doi.org/10.1074/jbc.M114.601484>
 37. Aki S, Yoshioka K, Takuwa N, Takuwa Y (2020) TGF β receptor endocytosis and Smad signaling require synaptojanin1-, PI3K-C2 α -, and INPP4B-mediated phosphoinositide conversions. *Mol Biol Cell*. <https://doi.org/10.1091/mbc.E19-11-0662>
 38. Takuwa Y (2003) Regulation of the Rho signaling pathway by excitatory agonists in vascular smooth muscle. *Adv Exp Med Biol* 538:67–75
 39. Takuwa Y, Yoshioka K, Takuwa N, Wang Y, Azam MA, Sugimoto N (2005) Calcium-dependent regulation of Rho and myosin phosphatase in vascular smooth muscle. *Biomed Rev* 16:13–21

Publisher's Note

Springer Nature remains neutral with regard to jurisdictional claims in published maps and institutional affiliations.